Supporting information for

Tailored thermally stable functionalization of $CsPbBr_3$ nanocrystals for polymer nanocomposite scintillator fabrication

Jan Král,[a,b*] Kateřina Děcká,[a] Petr Liška,[c,d] Solangel Rojas Torres,[a] Jan Valenta,[e] Vladimir Babin,[b] Ildefonso León Monzón,[f] Václav Čuba,[a] Eva Mihóková,[a,b] and Etiennette Auffray[g]

[a] *Faculty of Nuclear Sciences and Physical Engineering, Czech Technical University in Prague, Břehová 7, Prague 115 19, Czech Republic. Email:kralja13@fjfi.cvut.cz*
[b] *Institute of Physics of the Czech Academy of Sciences, Cukrovarnická 10, Prague 162 00, Czech Republic.*
[c] *Institute of Physical Engineering, Faculty of Mechanical Engineering, Brno University of Technology, Technická 2896/2, 616 69 Brno, Czech Republic.*
[d] *Central European Institute of Technology, Brno University of Technology, Purkyňova 656/123, 612 00 Brno, Czech Republic.*
[e] *Faculty of Mathematics and Physics, Charles University, Ke Karlovu 3, 121 16 Prague, Czech Republic.*
[f] *Faculty of Physical-Mathematical Sciences, Autonomous University of Sinaloa, Culiacán 80000, Mexico.*
[g] *CERN, Esplanade des Particules 1, Meyrin 1211, Switzerland*

Influence of hydrolysis on AHFS ligand exchange

In Fig. 1, there is comparison of $CsPbBr_3$ nanocrystals after ligand exchange performed with AHFS freshly dissolved in water and with AHFS dissolved in water for 2 hours. One can see, much greater extent of ligand exchange and surface pasivation of nanocrystals by AHFS with freshly prepared solution compared to 2 hours old solution evidenced by relatively lower signal from C-H vibrations around 2900–3000 cm^{-1} and stronger signal from AHFS specific vibrations as shows comparison with pure AHFS powder. The explanation of this difference is most probably hydrolysis of AHFS in water over time decreasing pure AHFS concentration by forming silanol and siloxane oligomers and polymers.

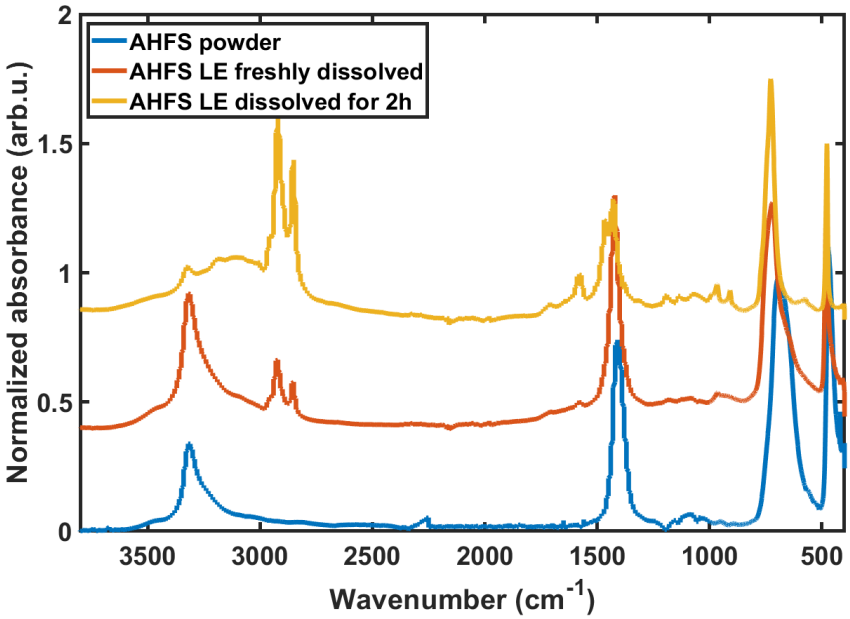

Figure 1: FTIR spectra of samples after AHFS ligand exchange with freshly prepared and aged AHFS in water.

PL and RL decay curves

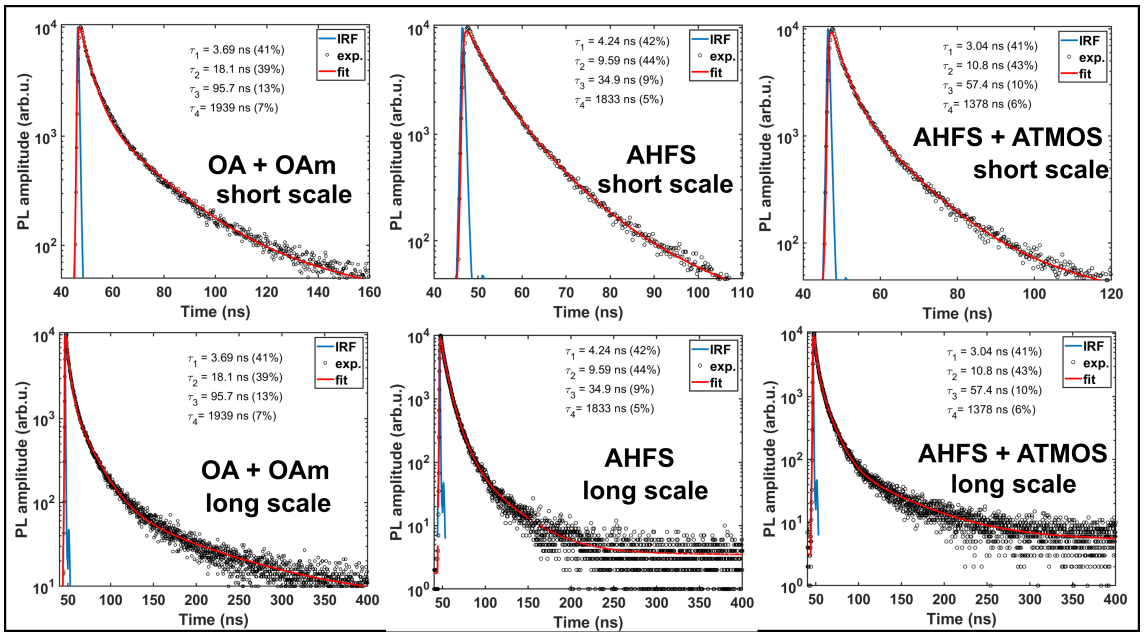

Figure 2: PL decay curves at different stages of nanocrystal allyl-functionalization presented in two scales, short above and long below. The experimental data are represented by black circles, 4-exponential fit is red line and IRF is blue line. Inset: determined decay components and their contribution.

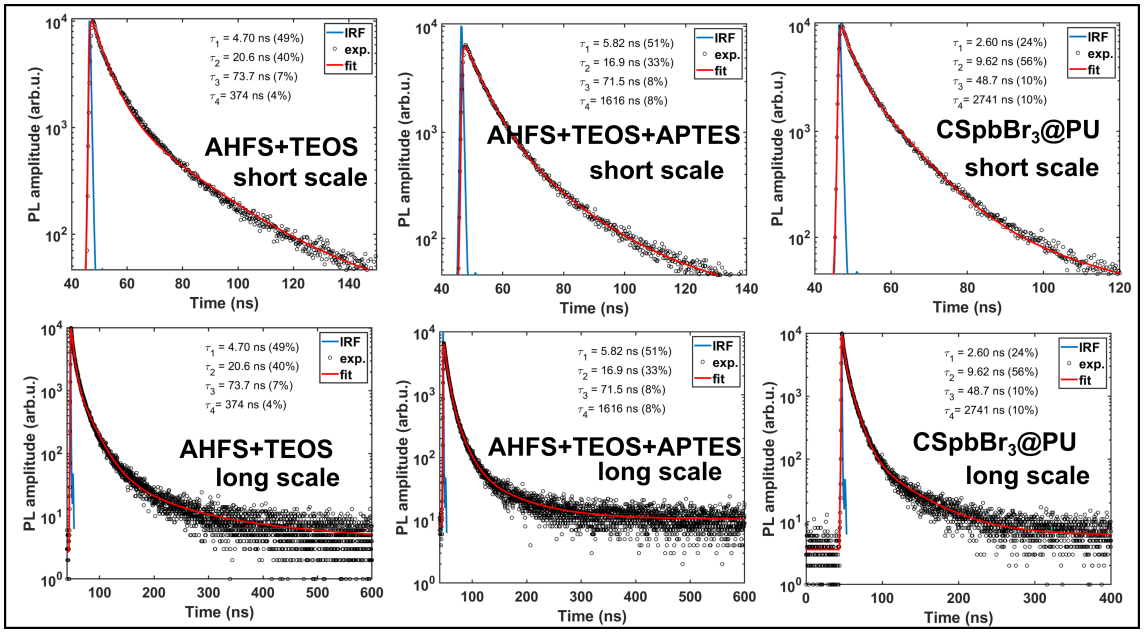

Figure 3: PL decay curves at different stages of nanocrystal amino-functionalization and PL decay of $CsPbBr_3$ PU nanocomposite, all presented in two scales, short above and long below. The experimental data are represented by black circles, 4-exponential fit is red line and IRF is blue line. Inset: determined decay components and their contribution.

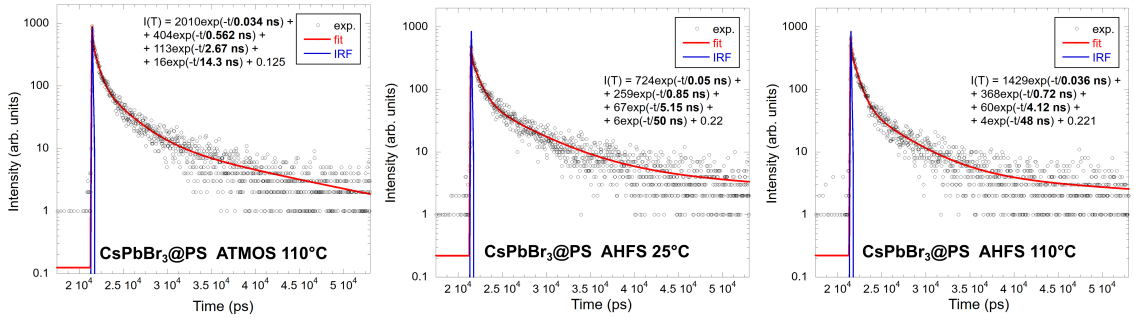

Figure 4: RL decay curves of polystyrene nanocomposites with only ATMOS functionalized nanocrystals prepared at 110°C and with fluoride treated nanocrystals prepared at 25°C and 110°C. The experimental data are represented by black circles, 4-exponential fit is red line and IRF is blue line. Inset: determined decay components and their contribution.

Nanocomposite stability over time

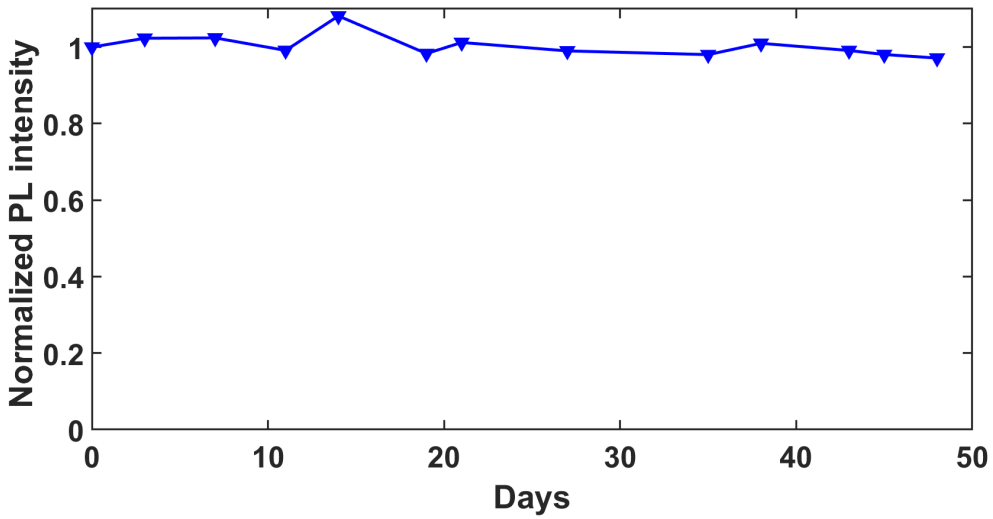

Figure 5: Relative PL intensity of $CsPbBr_3$ polystyrene nanocomposite over time. Stored in the dark under normal atmosphere.

SiO_2 corpuscles composition and influence of the e-beam

Acquired EDX spectrum of $CsPbBr_3$ nanocrystals embedded in SiO_2 using TEOS from Fig. 4b) of the article are Fig. 6a). It shows, that the wider corpuscles consist of SiO_2 and contains cs, Pb, Br, however, not in a correct stoichiometric ratio, with very low relative concentration of Br around 1.4% and 6:1 relative concentration of Pb:Cs. We explain this discrepancy due to utilization of relatively low-energy electron beam for the EDX measurements (15 keV), which significantly decreases reliability of the relative concentration for the heavier elements, especially Pb and Br. Moreover, we have observed significant damage over time induced in the NCs due to radiolysis. Therefore, the elevated amount of Pb in comparison to Cs and very low relative concentration of Br is a combination of several factors, including the fact that the NCs upon disintegration from radiolysis tend to form individual metallic Pb nanoparticles (Dang et al., 2017). The influence of the acquired electron beam dose on the $CsPbBr_3$ nanocrystals is demonstrated in Fig. 6b)-d). The dark contrast of the nanocrystal cubes changes after few seconds of the e-beam influence to bright and dark spots, presumably Pb particles, are formed. After prolonged exposure, only small spherical particles consisting most probably of lead are observable.

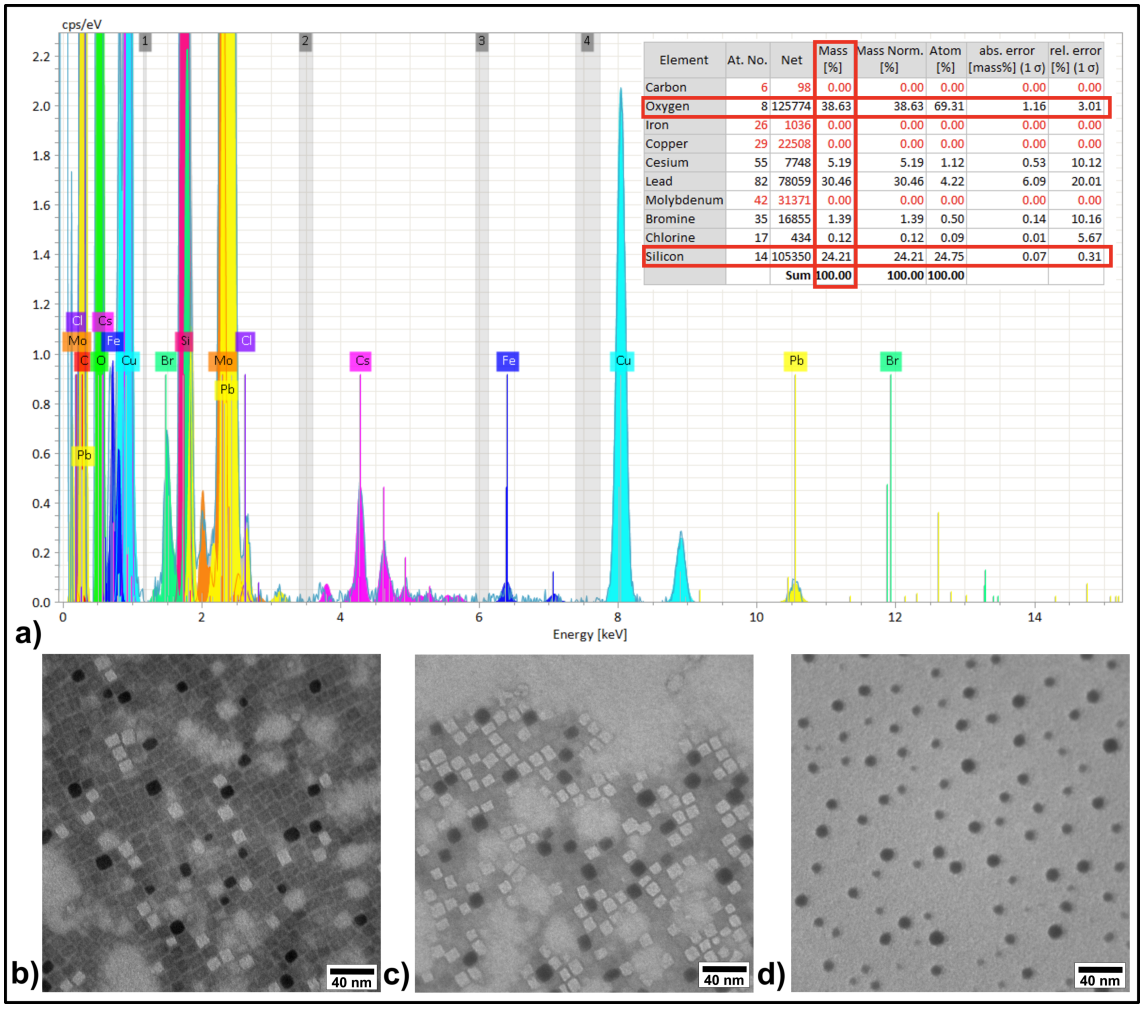

Element	At. No.	Net	Mass [%]	Mass Norm. [%]	Atom [%]	abs. error [mass%] (1 σ)	rel. error [%] (1 σ)
Carbon	6	98	0.00	0.00	0.00	0.00	0.00
Oxygen	8	125774	38.63	38.63	69.31	1.16	3.01
Iron	26	1036	0.00	0.00	0.00	0.00	0.00
Copper	29	22508	0.00	0.00	0.00	0.00	0.00
Cesium	55	7748	5.19	5.19	1.12	0.53	10.12
Lead	82	78059	30.46	30.46	4.22	6.09	20.01
Molybdenum	42	31371	0.00	0.00	0.00	0.00	0.00
Bromine	35	16855	1.39	1.39	0.50	0.14	10.16
Chlorine	17	434	0.12	0.12	0.09	0.01	5.67
Silicon	14	105350	24.21	24.21	24.75	0.07	0.31
		Sum	100.00	100.00	100.00		

Figure 6: a) EDX spectrum of $CsPbBr_3$ nanocrystals embedded in SiO_2 from Fig. 4b) of the article, inset table of measured composition. b) TEM image of the NCs right after focusing of the e-beam. c) TEM image after several seconds of the e-beam influence. d) TEM image after prolonged exposure

References

Z. Dang, J. Shamsi, F. Palazon, M. Imran, Q. A. Akkerman, S. Park, G. Bertoni, M. Prato, R. Brescia, and L. Manna. In situ transmission electron microscopy study of electron beam-induced transformations in colloidal cesium lead halide perovskite nanocrystals. *ACS Nano*, 11(2):2124–2132, Feb. 2017. ISSN 1936-086X. doi: 10.1021/acsnano.6b08324. URL `http://dx.doi.org/10.1021/acsnano.6b08324`.